

REPRESENTING TWENTIETH CENTURY SPACE-TIME CLIMATE VARIABILITY.

II: DEVELOPMENT OF 1901-1996 MONTHLY GRIDS OF TERRESTRIAL SURFACE

CLIMATE

Mark New^{*}, Mike Hulme and Phil Jones

Climatic Research Unit, School of Environmental Sciences, University of East Anglia

Norwich, NR4 7TJ, United Kingdom

Submitted, *Journal of Climate*, 8 July, 1998

ABSTRACT

The authors describe the construction of a 0.5° latitude/longitude gridded dataset of monthly terrestrial surface climate over for the period 1901-1996. The dataset comprises a suite of 7 climate elements: precipitation, mean temperature, diurnal temperature range, wet-day frequency, vapour pressure, cloud cover and ground-frost frequency. The spatial coverage extends over all land areas, excluding Antarctica. Fields of monthly climate anomalies, relative the 1961-1990 mean, were interpolated from surface climate data. The anomaly grids were then added to a 1961-1990 mean monthly climatology (described in Part I) to arrive at grids of monthly climate.

The *primary variables*, precipitation, mean temperature and diurnal temperature range, were interpolated directly from station observations. The resulting time-series are compared with other, coarser resolution, datasets of similar temporal extent. The remaining climatic elements, termed *secondary variables*, were interpolated from merged datasets, comprising station observations and, in regions where there were no station data, synthetic data estimated using predictive relationships with the primary variables, which are described and evaluated.

It is argued that this new dataset represents an advance other products because (i) it has higher spatial resolution than other datasets of similar temporal extent, (ii) it has longer temporal coverage than other products of similar spatial resolution; (iii) it encompasses a more extensive suite of surface climate variables than available elsewhere and (iv) the construction method ensures that strict temporal fidelity is maintained. The dataset is available from the Climatic Research Unit.

1. Introduction

The description of the mean state and variability of recent climate is important for a number of purposes in global change research. These include monitoring and detection of climate change, climate model evaluation, calibration or merging with satellite data, biogeochemical modelling and construction of climate change scenarios (New *et al.*, in press). Datasets of surface climate which describe variability in space and time (Hulme, 1992; Jones, 1994; Easterling *et al.*, 1997) have historically had incomplete spatial coverage and been of coarse resolution ($>2.5^\circ$ latitude/longitude). This is because their primary purposes, climate change detection and General Circulation Model (GCM) evaluation, do not necessarily require spatially continuous fields or higher resolution.

There has been a growing demand for datasets with high spatial (e.g. 0.5° latitude/longitude) and temporal (e.g. monthly or daily) resolution that are also continuous over the space-time domain of interest. Potential applications for such datasets include understanding the role of climate in biogeochemical cycling (Dai and Fung, 1993; Cramer and Fischer, 1996), climate change scenario construction (Carter *et al.*, 1994) and high-resolution climate model evaluation (Christensen *et al.*, 1997). Yet there are currently few datasets that satisfy the requirement of high spatio-temporal resolution. Notable exceptions are the monthly time step Global Precipitation Climatology Project (GPCP) data set (Xie and Arkin, 1996; Xie *et al.*, 1996), the monthly 1900-1988, 2.5° latitude/longitude precipitation dataset of Dai *et al.* (1997a), and the 0.5° latitude/longitude daily dataset being developed by Piper and Stewart (henceforth PS, 1996). However these products either cover relatively short periods (1970's to present - GPCP, PS), are limited to precipitation (GPCP, PS, DAI) and minimum and maximum temperature (PS), do not include an elevation dependence in their interpolation schemes (GPCP, PS, DAI), or have a relatively coarse resolution (DAI). A further limitation is that GPCP and PS interpolate directly from station time series: their methodology has to overcome difficulties in interpolating monthly climate over complex terrain and they cannot make use of the more extensive network of station climatological normals to define a mean climatology (see below).

In this paper, we describe the construction of a new dataset of monthly surface climate over global land areas, excluding Antarctica, for the period 1901-1996. The dataset is gridded at 0.5° latitude/longitude resolution and comprises a suite of seven variables, namely, precipitation, wet-day

frequency, mean temperature, diurnal temperature range, vapour pressure, cloud cover and ground-frost frequency.

In constructing the monthly grids we used the anomaly approach which attempts to maximise available station data in space and time (New *et al.*, in press). In this technique, grids of monthly anomalies relative to a standard normal period (in our case 1961-1990) were first derived. The anomaly grids were then combined with a high-resolution mean monthly climatology to arrive at fields of estimated monthly surface climate. We used the 0.5° latitude/longitude 1961-1990 climatology described in a companion paper (Part I; New *et al.*, in press) for this purpose

The advantage of this approach is that the number of archived *and* easily obtainable station normals is far greater than that of station time series, particularly as one goes back in time. Using as many stations as possible to generate the mean fields, together with an explicit treatment of elevation dependency, maximises the representation of spatial variability in mean climate. Monthly anomalies, on the other hand, tend to be more a function of large-scale circulation patterns and relatively independent of physiographic control. Therefore, a comparatively less extensive network is sufficient to describe the month-to-month departures from the mean climate.

We have divided the seven climatic elements into two groups, *primary* and *secondary* variables. The former, comprising precipitation, mean temperature and diurnal temperature range, were considered to have sufficient station coverage to attempt the derivation of grids directly from station anomalies for the entire period 1901-1996. The interpolation of the primary variable anomaly grids is covered in the first half of the paper. We also compare our datasets over a few selected regions with some other earlier long-term gridded data.

The networks of stations with time series of secondary variables, namely wet-day frequency, vapour pressure, cloud cover and ground frost frequency, were insufficient for derivation of anomaly fields directly from station data. We therefore used empirical relationships to derive *synthetic* anomalies from the gridded anomalies of primary variables and merge these with station anomalies of secondary variables over regions where such data are available. The merged anomalies were then applied to the 1961-1990 normal grids mentioned above, thereby standardising the anomalies against high resolution observe data. This approach is described in more detail in the second half of the paper, along with an evaluation of the various empirical relationships.. We end the paper with some discussion and conclusions.

2. Primary variables

a. Datasets

Three global station datasets compiled by the Climatic Research Unit (CRU) form the basis for the construction of the gridded anomalies of primary variables. The precipitation (Eischid *et al.*, 1991; Hulme, 1994, updated) and mean temperature (Jones, 1994, updated) station data have been compiled by CRU over the last 20 years. The diurnal temperature range dataset is based on the Global Historical Climatology Network (GHCN) maximum and minimum temperature data (Easterling *et al.*, 1997), but has been updated for more recent years by CRU, and enhanced with additional station data obtained by CRU and the UK Meteorological Office (Horton, 1995). The original data have been subjected to comprehensive quality control over the years as described by the above authors. Updates for more recent years and additional station data collated by CRU have also been checked for homogeneity and outliers.

The station networks for all three variables exhibit a gradual increase in the total number of stations from 1901 to about 1980, after which numbers decline (Figures 1-3) The recent reduction in numbers is primarily in areas with good or reasonable station coverage. However, the spatial coverage of stations reporting diurnal temperature range shows a more serious reduction in the 1990s. This should in due course be alleviated by the inclusion of mean-monthly maximum and minimum temperature in the post-1995 monthly CLIMAT reports, and once updated datasets for the former USSR and China are included in the CRU dataset.

The station density required to adequately describe monthly spatial variability is characteristically greater for precipitation than diurnal temperature range and mean temperature. For example, Dai *et al.* (1997a) found that zonally averaged inter-station correlation distances for annual precipitation fall to an insignificant level (~ 0.36 for $N=30$) at 200km for 0° - 30° N, 400km for 30° N- 60° N, 300km for 60° N- 90° N, 550km for 0 - 30° S and 800km for 30° S- 60° S. This compares to distances of between 1200km and 2000km for mean temperature reported by Hansen and Lebedeff (1987) and Jones *et al.* (1997).

We build on the approach of Dai *et al.* (1997) and define the correlation decay distance (CDD) as the distance at which zonally averaged inter-station correlation is no longer significant at the 95% level (~ 0.36 for $N=30$). Our own analyses, using station records with at least 30 years of data, indicate

that the larger CDDs in the Southern Hemisphere reported by Dai *et al.* (1997a) do not occur when monthly precipitation anomalies are considered (Figure 4). Indeed, we find similar CDDs for comparable latitude bands in the Northern and Southern Hemispheres (350-400km for 0-30°N/S, and 400-500km for 30-60°N/S), although northern CDDs are noticeably shorter in the NH summer. In addition CDDs exhibit seasonality, particularly in the case of temperature where winter CDDs are much greater than in summer (Jones *et al.*, 1997). Diurnal temperature range CDDs are intermediate between those of precipitation and mean temperature.

We use globally averaged CDDs for each variable during the interpolation of monthly anomaly grids described in the next section.

b. Anomaly interpolation

Prior to interpolation each station time-series was converted to anomalies relative to the 1961-1990 mean. Series with less than 20 years of data during 1961-1990 were excluded from the analysis. Anomalies for all three variables were expressed in absolute units. Other transformations of precipitation are possible, such as percentage of mean, standard deviation (Jones and Hulme, 1996) or expression in terms of some other distribution (Diaz *et al.*, 1989; Hutchinson, 1995b). Of all these, absolute units and percentage anomalies are the simplest, particularly because the re-expression into absolute monthly units requires only a mean field. We used absolute units because of the potential problems arising from the interpolation of percentage anomalies from stations in arid regions, where relatively small absolute precipitation anomalies can produce quite large relative (percent) anomalies.

After conversion to anomalies the precipitation data were transformed to a “signed log” format, as follows:

$$\begin{aligned}
 a_{sl} &= \log(|a|) & a > 0 \\
 &= -\log(|a|) & a < 0 \\
 &= 0 & a = 0
 \end{aligned}
 \tag{1}$$

Back-transformation of the interpolated grid to produce absolute departures was then a simple process. This helped prevent the interpolation of steep gradients derived from two adjacent stations into nearby regions with no station control. This can happen where two stations are on opposite sides of an orographic barrier. For example, on many Caribbean Islands northern coasts are several times wetter than southern coasts and resulting anomalies (in mm units) exhibit similar contrasts.

We used thin-plate spline interpolation to interpolate the monthly station anomalies to a regular 0.5° latitude/longitude grid. Thin-plate splines are described elsewhere (Wahba, 1990; Hutchinson and Gessler, 1994; Hutchinson, 1995a) and the details are not repeated here. As with many other geostatistical interpolation techniques, the variable of interest can be interpolated as a function of longitude, latitude and any of a number of topographic parameters such as elevation and aspect. Most of the spatial variation in monthly temperature anomalies is independent of topography and interpolation as a function of only latitude and longitude is sufficient. This is not true for precipitation, where inclusion of elevation as a co-predictor has been shown to improve the accuracy of the anomaly interpolation (M. F. Hutchinson, personal communication, 1997). However, the inclusion of elevation as a predictor invokes a penalty by markedly reducing the degrees of freedom available for defining the fitted surface. It was only over Europe, USA and southern Canada that there were sufficient stations to justify the use of elevation.

Computation times for the spline-fitting increase exponentially with the number of stations, so separate interpolations were carried out over several overlapping geographic tiles (e.g. Figure 5). The tiles were then merged to produce global anomaly fields, using the same technique as New *et al.* (in press) used in the construction of their 1961-1990 mean fields.

As discussed earlier, a station is unlikely to provide useful information about the variable of interest at grid-points beyond its CDD. To prevent extrapolation to unrealistic values the interpolated anomaly fields were forced towards zero at grid-points beyond the influence of any stations. This was accomplished by including input data stations with values of zero in regions where there were no stations within a predefined distance, chosen to be equal to the global mean CDD. These distances were 450km for precipitation, 750km for diurnal temperature range and 1200km for mean temperature. Figures 1-3 show for selected years, the areas where there are not any stations within these distances. Although globally averaged CDDs were used, there is scope for the application of latitudinally or spatially varying CDDs and this will be considered in future versions of the dataset.

c. Combination with climatology

We combined the interpolated anomaly fields for each month from 1901 to 1996 with the CRU 0.5° 1961-1990 mean monthly climatology (New *et al.*, in press) to arrive at monthly grids of surface climate. This combined dataset is henceforth referred to as CRU05. The CRU 1961-1990 climatology

was constructed with this purpose in mind, and has a number of advantages over other climatologies. Chief among those is that it is strictly constrained to the period 1961-1990. This permitted the addition of the anomaly fields, which were standardised against the 1961-1990 period, without any biases arising from temporal sampling mismatches. The CRU climatology is also the only published climatology of global land areas which encompasses the necessary range of climate elements.

In some areas with sparser station coverage, the 1961-1990 average of the monthly anomaly grids diverged from zero, for example over Angola and the Democratic Republic of the Congo. This arose directly from the interpolation error in the individual anomaly fields which, not unexpectedly, did not sum to zero. To maintain consistency, individual fields from 1961-1990 were adjusted so that their 1961-1990 mean was zero by subtracting this mean interpolation error.

It should be noted that a direct consequence of the relaxation of the anomaly surfaces to zero in regions with no data coverage is that the resulting monthly climate relaxes towards the 1961-1990 climatology in such areas. This is discussed in more detail elsewhere in the paper.

d. Evaluation

Major sources of error in gridded datasets of this nature are instrumental (isolated errors, systematic error and inhomogeneity), inadequate station coverage and interpolation errors (Groisman *et al.*, 1991; Dai *et al.*, 1997a; Jones *et al.*, submitted). Isolated errors and subtle inhomogeneities not detected during quality control do not have a significant effect at the regional scale. However, such errors are noticeable at grid-points near to the offending station, particularly if the network is sparse. Inadequate station coverage is the largest source of error, but there is little that can be done about this except to ensure that the existing data are error free and that the interpolation methodology makes maximum use of the available data. We believe that thin-plate splines achieve this by including gradients and, where data permit, by using three-dimensional interpolation.

Extensive evaluation of the CRU05 gridded data is beyond the scope of this paper. An intercomparison of CRU05 precipitation and several other long-term instrumental and shorter term satellite and/or gauge based datasets is the focus of a separate study (Hulme *et al.*, in preparation). In this section a limited comparison with two precipitation, one mean temperature and one diurnal temperature range dataset is presented to highlight the differences that can arise due to either differing station networks and/or interpolation approaches.

1) PRECIPITATION

Regional time-series derived from CRU05 and two other precipitation datasets were compared over two regions with good and poor station coverage respectively, the UK (49N, 11W – 61N, 3E) and the Amazon basin (15S, 70W – 5N, 40W). The other two datasets are those of Hulme (1994) and Dai *et al.* (1997a), both of which have a spatial resolution of 2.5° lat/lon (henceforth HULME and DAI, respectively). These were the only two other global datasets of monthly precipitation covering the period 1901-1996 which were known to the authors. Both these datasets were produced by interpolation of station anomalies, using a Thiessen polygon (HULME) and spherical inverse-distance weighted approach (DAI) respectively. While HULME grid-points are estimated using only those within the grid-box, DAI employ an influence radius of 350km to select data. However, HULME uses a spherical angular distance weighting with an influence radius of 600km to infill missing data at individual stations *prior* to the Thiessen-gridding process.

Area-averaged time-series for the two regions were constructed using the approach recommended by Jones and Hulme (1996). Grid-point data were transformed to anomalies from the 1961-1990 mean, expressed in standard deviation units. These were then averaged, with a latitudinal weighting, and back-transformed to mm units using the regionally-averaged 1961-1990 monthly means and standard deviations. The CRU05 dataset was first regrided to 2.5° resolution, again using a latitudinal weighting. Both DAI and CRU05 were masked using HULME, ensuring that these more spatially complete datasets do not have more grid-points than HULME. In fact, the masked DAI grids had fewer grid-points than HULME because (i) the DAI land-sea mask is slightly different to that of HULME and (ii) at the beginning and end of the record, DAI had fewer contributing stations than HULME, resulting in fewer grid-points with data.

The resulting regional time-series of annual precipitation, expressed as anomalies relative to the 1901-1996 mean, are shown in Figure 6. In both regions, the three datasets agree in broad detail, but exhibit some differences. Most notably, the CRU05 time-series have lower variance than the other two. This is accentuated in periods where there are fewer stations contributing to the construction of the HULME and CRU05 grids (and presumably also DAI). This is particularly so from 1901 to 1930 over the Amazon, where HULME and DAI exhibit a trend of increasing inter-annual variance back in time. The inter-annual variance at individual stations within the Amazon window was examined to determine

if this was a real signal or an artefact of the gridding process in HULME and DAI. For each of the 43 stations with records starting on or before 1915, 20-year running coefficients of variation (CV; i.e. running standard deviation / running mean) were calculated. The mean of these, plotted in Figure 6, does not exhibit the trend shown by DAI and HULME, leading to the conclusion that at least some of their increasing variance is a gridding artefact. Thus the CRU05 time-series appears more stable in the Amazon over the entire period, suggesting that either (i) interpolation to a continuous surface using splines is less sensitive to sparse station networks or (ii) interpolation to a finer grid prior to calculation of regional time-series is more robust, or both.

Figure 6 also provides a qualitative indication of the error that may be potentially associated with gridded precipitation datasets. All three have been generated using datasets that have many stations in common, but with different interpolation methods. Where the station network is poor, the different interpolation methods can produce quite varied results. Where the network is good, the three datasets tend to converge, but the splines produce regional time-series with lower inter-annual variance.

2) MEAN TEMPERATURE

Annual time-series of mean temperature were calculated from the CRU05 dataset and that of Jones (1994; updated; henceforth JONES) for the same two regions (Figure 7) and in the same way as precipitation (see above), except that the gridded data were transformed to absolute rather than standard deviation anomalies. The station network is sparse over the Amazon, with a maximum of 25 stations, but dropping off to two (JONES) and between six and seven (CRU05) before 1950. Although the two series are well correlated, CRU05 is less variable and diverges (warm offset) quite markedly from JONES before 1950. This is primarily due to there being fewer stations in JONES: annual time-series for the Amazon produced by Victoria *et al.* (1998) from a similar set of stations to CRU05 agree better with CRU05 than JONES over this period (not shown). Over the period with relatively good station coverage (1950-1990) the variability of JONES increases markedly while that of CRU05 remains relatively constant. Changes in the variance of both grid-box and regional time-series of temperature is to be expected in the method used by JONES (see discussion in Jones *et al.* 1997), while the CRU05 methodology is less sensitive to varying station networks.

The UK time-series from each dataset are very similar, although CRU05 is slightly warmer than JONES over 1930-1960. This is most likely because JONES has specifically excluded several stations

that exhibit marked urban warming (e.g. Dublin Airport and Kew) which are used in CRU05. The effect of these stations is diluted after 1960 when ~100 additional UK stations come into the CRU05 dataset. Inter-annual variability of the two series is also very similar, although CRU05 tends to have slightly lower variance after 1960 when the number of stations increases to over 100 (*c.f.* ~20 for JONES). As with precipitation, this example indicates that the two gridding methodologies converge with increasing station coverage.

On a hemispheric and global basis CRU05 agrees well with JONES. The major differences between the two occur before about 1940 (Figure 8), with CRU05 being about 0.1°C warmer and 0.1-0.2°C cooler than JONES in the Northern and Southern Hemispheres, respectively. Hemispheric averages are subject to some uncertainty due to sampling errors. Jones *et al.* (1997) have recently quantified these errors, which increase in the past when station coverage was sparser. In Figure 8 the standard errors are shown as a shaded band, calculated using the approach of Jones *et al.* (1997), but limited to the land domains under study here. To achieve this the Jones *et al.* (1997) 5°x5° grid-box standard errors were averaged over the domain of interest using their Equations 11 and 12. The number of spatial degrees of freedom was reduced by one-third (one-half) for the Northern (Southern north of 60°S) Hemisphere, to allow for the degrees of freedom that occur over the (excluded) ocean. It can be seen from Figure 8 that it is only at the very beginning of the century that the CRU05 masked time-series are more than one standard error different from JONES.

The differences between CRU05 and JONES are partly related to the extrapolation to data-sparse regions where CRU05 is relaxed towards the (warmer) 1961-1990 mean when there are no stations within the correlation decay distance. This is supported, in both hemispheres, by the larger positive offset associated with the time-series calculated from the full CRU05 grid.

However, the relaxation to the 1961-1990 mean does not explain the negative bias in the masked CRU05 series in the Southern Hemisphere. In this case, the offset may be due to the use of different (but overlapping) station networks. JONES is constructed using time-series where urban warming bias is minimal, whereas CRU05 makes use of all available station data. In earlier years over the Southern Hemisphere urban stations make a greater relative contribution to the CRU05 network and result in a larger negative offset. This effect is not as marked in the Northern Hemisphere because of the more extensive network of non-urban stations and the fact that urban warming was already underway to some extent in the first half of the century.

3) DIURNAL TEMPERATURE RANGE

Northern Hemisphere time series derived from CRU05 were compared to those derived from the dataset of Easterling *et al.* (1997; henceforth EAST) for the period 1950-1993 (Figure 9). Note that the CRU05 series is constructed using the full Northern Hemisphere fields because there was no information on the space-time distribution of grid-boxes with data in EAST. Both series show the marked decreasing trend from 1950-1993 reported by EAST, though CRU05 does not show as large a negative anomaly as EAST in 1993; this is, however, the year with sparsest station coverage in both datasets. Prior to 1940, the CRU05 record is dominated by station data in North America and Russia and shows a similar trend to the combined long-term records from these regions reported by Karl *et al.* (1993) for these regions. Some of the decrease in CRU05 prior to 1940 is also due to the relaxation towards the 1961-1990 mean (lower) in regions that have no station control, but nonetheless contribute to the hemispheric mean.

3. Secondary variables

a. Datasets

The datasets of secondary variables (wet-day frequency, vapour pressure, cloud cover and ground frost frequency) held by CRU are less comprehensive than those of the primary variables. This is partly because CRU has only recently made efforts to obtain these variables, but also because they are not as widely measured than temperature and precipitation, particularly in earlier years. To date, station time series for some or all of the secondary variables have been acquired from some 70 different sources. Several of these are public domain or available for purchase, but many have been obtained through personal contacts or directly from National Meteorological Agencies (NMAs). These datasets are updated on an *ad hoc* basis as new data are obtained, and more regularly with monthly CLIMAT reports (wet-day frequency, vapour pressure and sunshine).

The distribution of stations in the CRU dataset from 1901-1995 is shown in Figures 10-12. Cloud cover over the northern mid-high latitudes is fairly comprehensive from the 1950s onwards, but is virtually non-existent elsewhere, except for the 1980s where the Hahn *et al.* (1994) global synoptic station dataset makes a major contribution. This will be significantly enhanced when the updated (1950s-1995) Hahn synoptic data are released in 1998 (Carole Hahn, personal communication, 1998).

The distribution of vapour pressure and wet-day frequency stations exhibits a similar pattern to that of cloud cover, but does not benefit from the inclusion of synoptic data in the 1980s or data from the USA (efforts are currently underway to obtain long-term USA data), Western Europe, China (for vapour pressure) and Australia. Both these datasets will be enhanced once data from the Monthly Climatic Data for the World / CLIMAT are incorporated, a process that is at present underway.

Station data for ground frost frequency (not shown) are restricted to the former USSR, Canada, the UK and a few other locations where access to daily ground/grass minimum temperature permitted the calculation of these time series.

We calculated CDDs for cloud cover, vapour pressure and wet-day frequency at latitudes where the stations network permitted (Figure 13; 60°S-90°N for cloud cover, 0-90°N for wet-day frequency and 30°N-90°N for vapour pressure). Cloud cover CDDs range between 500km at mid-high latitudes and ~1000km at low latitudes, with a global average of ~750km. Vapour pressure exhibits similar CDDs to mean temperature, both in terms of distances (1000-2000km) and seasonal cycle, suggesting that the two are a function of the same large-scale circulatory forcings. Wet-day frequency decay distances are ~500km at low-mid Northern latitudes and ~300km at high Northern latitudes, mirroring the latitudinal variation of precipitation CDDs.

b. Empirical relationships with primary variables

The patchy distribution of stations with secondary variable data, particularly prior to 1960, meant that interpolation of anomalies directly from station data was not feasible. This is despite the large CDDs determined for cloud cover and, particularly, vapour pressure. We therefore used the existing data to develop and/or test empirical (in the case of cloud cover and ground frost frequency) or conceptual (vapour pressure and wet-day frequency) relationships with the primary variables. These relationships were used to calculate grids of *synthetic* monthly anomalies. In the case of cloud cover, wet-day frequency and vapour pressure, the synthetic grids were then blended with station anomalies in the regions where such data were available. Finally, the resultant anomaly fields were combined with the CRU 0.5° 1961-1990.

1) CLOUD COVER

The negative correlation between diurnal temperature range and both precipitation and cloud cover has been well documented at both regional/global scales (e.g. Karl *et al.*, 1993; Dai *et al.*, 1997) and at individual weather stations (e.g. Wang *et al.*, 1993; Ruschy *et al.*, 1991). We used this as the starting point for the development of a predictive relationship for cloud cover.

Station anomaly time series of cloud cover, precipitation and diurnal temperature range were grouped into 5° lat/lon bins. Monthly cloud cover in each bin was regressed on diurnal temperature range and precipitation. In general, cloud cover correlated better with diurnal temperature range than precipitation (Figure 14). The strong correlation between precipitation and diurnal temperature range (not shown) also meant that the inclusion of both climate elements in the regression resulted in little additional variation in cloud cover being explained. As a rule, correlation with diurnal temperature range is weak in arid regions due to a general absence of cloud cover. Notable exceptions were the arid west coasts of Africa and South America where low cloud/fog associated with advection is frequent. The relationship between diurnal temperature range and cloud cover is also weak at around 60°N in winter, and becomes positive in the Arctic. This is probably because the extreme cold and the absence of incoming solar radiation during high latitude winters results in minimal modulation of surface energy balance by cloud cover. At these high latitudes the correlation between precipitation and cloud cover is slightly stronger.

We discarded precipitation from further analysis because of the generally better relationship between diurnal temperature range and cloud cover. A further reason for using only one predictor variable arises from the way the grids of primary variables (which form the input in the calculation of synthetic fields) were produced. In years before ~1950 both precipitation and diurnal temperature range fields are forced towards the 1961-1990 mean in regions where there is no station control (discussed earlier). This occurs more frequently with diurnal temperature range than precipitation. Using a regression against diurnal temperature range *and* precipitation could produce unrealistic synthetic cloud values where one of the predictor variables is constrained to zero and the other not.

At each 5° lat/lon bin for which there were data we used resistant regression (Emerson and Hoaglin, 1983) to determine a predictive relationship with diurnal temperature range. Resistant regression is insensitive to isolated data errors, which is useful when the analysis is automated for a

large number of data samples. We then interpolated the monthly regression coefficients to a regular 0.5° lat/lon grid. The 0.5° lat/lon grids of diurnal temperature range anomalies were subsequently used as input to calculate synthetic cloud cover anomaly grids. We evaluated the resulting synthetic grids by degrading them to 2.5° lat/lon resolution and comparing them to the 1982-1991 monthly cloud cover grids of Hahn *et al.* (1994). Monthly grid-point correlations (not shown) for the ten years of data in common are similar to those in Figure 14 (top) indicating that the use of diurnal temperature range grids captures the majority of covariance between cloud cover and diurnal temperature range that occurs at individual stations.

Grid-point data from the synthetic anomaly grids were used as artificial station data in areas where there were no station control, defined as a distance further than 700km any observed data. Figure 15 provides an example of the resultant network of artificial and real stations. The combined station and synthetic data were interpolated using the method described in Section 2.b to produce anomaly grids at 0.5° lat/lon resolution and subsequently combined with the CRU05 climatological mean fields to produce monthly grids of cloud cover for 1901-1996.

Because diurnal temperature range is relaxed to the 1961-1990 mean in areas where there are no station data, the cloud cover grids exhibit similar behaviour. Thus, prior to 1950, over most regions in the Northern tropics and Southern Hemisphere the CRU05 cloud cover grids approach the 1961-1990 climatology and have little or no inter-annual variability.

2) VAPOUR PRESSURE

The relatively large CDDs for vapour pressure suggest that there is value in interpolating anomalies from station data where they are present and using synthetic data in regions without vapour pressure data.

The vapour pressure network was extended to include coverage over China, Sumatra and Bolivia by converting time series of monthly relative humidity and mean temperature to vapour pressure (e) using the standard formula of Shuttleworth (1992):

$$e_s = 6.108 \exp\left(\frac{17.27T}{237.3+T}\right) \text{ hPa} \quad (2)$$

$$e = RH \cdot e_s \quad (3)$$

T = Mean monthly temperature
 e_s = Saturated vapour pressure at T
 RH = relative humidity (fraction)

While recognising the problems inherent in converting monthly relative humidity to vapour pressure it was felt that the approach was justified because their expression as anomalies removes much of the systematic bias arising from the conversion and station data is preferable to the alternative, namely, synthetic data.

Minimum temperature can be used to estimate dew point temperature, and hence vapour pressure by substitution in (2). This has been justified because dew point temperature and night minimum temperature tend to come into equilibrium and dew point temperature remains relatively constant during the day (Kimball *et al.*, 1997). The assumption becomes unreliable in arid regions where condensation does not occur during night and minimum temperature consequently remains well above dew point temperature. Kimball *et al.* (1997) derived a method which utilises information about potential evaporation and precipitation to yield improved estimates of dew point temperature in arid regions:

$$T_{dew} = T_{min} \left[-0.127 + 1.121 \left(1.003 - 1.444EF + 12.312EF^2 - 32.766EF^3 \right) + 0.0006DTR \right] \quad (4)$$

$$EF = PE / PRE_{ann}$$

PE = daily potential evaporation

PRE_{ann} = annual precipitation

DTR = diurnal temperature range

Equation (4) was used to estimate dew point temperature and hence synthetic grid-point vapour pressure using equation (2). Two major differences in this approach to that of Kimball *et al.* (1997) are:

- it is used on mean monthly data while Kimball *et al.* (1997) used daily data to derive the relationship, and
- synthetic vapour pressure is subsequently converted to anomalies relative to the synthetic 1961-1990 mean.

The accuracy of the derived monthly estimates was evaluated using CRU monthly time-series of mean temperature, minimum temperature, precipitation and vapour pressure. Stations with common year-months of these variables were extracted and the vapour pressure estimated using (4) and (2). The estimated and observed vapour pressure were then standardised against their respective means and grouped into 5° lat/lon bins prior to calculation of comparative statistics on a month-by-month basis.

Correlation coefficients for January and July are shown in Figure 16 (other months are intermediate between these two). In general, the method works better in winter than in summer and, for any particular month, better at high latitudes than low latitudes. The method is least effective in arid regions, most notably central Asia and Northwest China, most probably for reasons discussed above. Results from China are subject to additional uncertainty arising from the conversion of observed relative humidity to vapour pressure.

A similar procedure to that used for cloud cover was followed to derive blended grids of monthly vapour pressure. Monthly grids of the primary variables were used in (4) and (2) to derive grids of synthetic vapour pressure. The synthetic values were converted to anomalies relative to the 1961-1990 synthetic mean. Synthetic grid-point data further than a CDD of 1000km from any observed station data were combined with the dataset of observed anomalies and interpolated using thin-plate splines. The resulting blended anomaly fields were added to the CRU05 1961-1990 mean climatology to arrive at monthly grids of surface vapour pressure for 1901-1996.

3) WET-DAY FREQUENCY

Synthetic values for wet-day frequency were calculated using the following conceptual relationship with precipitation:

$$WD = (a \cdot PRE)^x \quad (5)$$

where

$$a = \frac{(WD_n)^{1/x}}{PRE_n} \quad (6)$$

and

$$x = 0.45$$

WD = estimated wet - day frequency

PRE = monthly precipitation

WD_n = 1961–1990 mean monthly wet - day frequency

PRE_n = 1961–1990 mean monthly precipitation

Defining a as in (6) forces predicted wet-day frequency to equal the 1961-1990 mean when monthly precipitation is equal to the 1961-1990 mean precipitation (Figure 17). A value of 0.45 for x in (5) was chosen by selecting the value that resulted in the smallest mean absolute error between

predicted and observed wet-day frequency in the CRU dataset of station time-series. At individual stations the optimum value of x varied between ~ 0.35 and ~ 0.6 . Synthetic wet-day frequency values were constrained to be zero if there was no observed precipitation and always to be no greater than the number of days in the month.

The accuracy of the relationship was assessed using observed time-series of precipitation and wet-day frequency in the CRU station dataset. The correlation between observed and predicted varies between 0.35 and 0.96 (Figure 18; Figure 19). The correlation is better in humid than in sub-humid regions and, at most stations, better in winter than in summer, where precipitation tends to be more frontal than convective. Predictive error exhibits a trend from positive bias at low observed wet-day frequency to negative bias at high observed wet-day frequency (Figure 19). This is partly a function of the formulation of (5) and the upper limit (number of days in month) for synthetic wet-day frequency. Thus at an observed frequency of one, the error cannot be less than minus one, but can have any positive value, leading to an overall positive bias. Conversely, when the observed frequency is equal to the number of days in the month, positive errors are not possible, resulting in an overall negative bias.

As with the other secondary variables, the synthetic anomaly fields were merged with observed station anomalies and combined with the 1961-1990 climatology to arrive at grids of monthly wet-day frequency from 1901 to 1996.

4) GROUND FROST FREQUENCY

There are very few ground frost frequency station data in the CRU dataset. Consequently, a purely empirical approach was used to generate monthly grids of this variable. Previous work had identified a good predictive relationship between *mean* monthly ground frost frequency and minimum temperature (New *et al.*, in press). Re-analysis of the data used by New *et al.* (in press) resulted in an improved prediction:

$$\begin{aligned} F &= 100 & T_{mn} &\leq -14 \\ F &= 50 + 50 \cdot \cos[7.5(T_{mn} + 14 - DT_{mn})] & -14 &< T_{mn} < 10 \\ F &= 0 & T_{mn} &\geq 10 \end{aligned} \quad (7)$$

where

$$DT_{mn} = 0.32 \cdot |12 - |T_{mn} + 2||$$

F = estimated ground - frost frequency in percent

T_{mn} = minimum temperature in Celsius

The suitability of (7) for predicting monthly ground-frost frequency was tested against observed monthly time-series from 120 stations in the UK (Figure 20). Most of the predictions are within $\pm 10\%$ of the observed values, with a tendency for over and under-estimation at low and high observed frequencies respectively. Reasons for this are essentially the same as those producing a similar pattern for wet-day frequency. Observed-predicted correlations are lowest in summer because, at any station, there are few months with both observed and simulated frost days greater than zero.

For the calculation of monthly ground-frost frequency fields, (7) was used with gridded minimum temperature (i.e. mean temperature minus one-half diurnal temperature range) to generate synthetic ground-frost frequency anomaly fields. These were subsequently added to the CRU05 climatology to arrive at monthly ground-frost frequency grids in absolute units for 1901-1995. Thus, ground-frost frequency is the only secondary variable derived entirely from synthetic anomalies and not merged with observed station data.

4. Conclusions

We have described the construction of a *spatially complete* gridded dataset of monthly surface climate comprising seven variables over global land areas for the period 1901-1996. These data represent an advance over previous products for several reasons.

- The dataset has a higher spatial resolution (0.5° latitude by longitude) than other datasets of similar temporal extent.
- Conversely, it extends much further back in time than other products that have similar spatial resolution.
- It encompasses a more extensive suite of surface climate variables than available elsewhere, namely: mean temperature and diurnal temperature range, precipitation and wet-day frequency, vapour pressure, cloud cover and ground-frost frequency.
- The construction method ensures that strict temporal fidelity is maintained: the anomalies are calculated using the same 1961-1990 period as the mean climatology to which they are applied.

These time-series are of particular use in applied climatology, as spatially continuous input data to environmental models. Examples include modelling biogeochemical cycling in terrestrial ecosystems and global/regional hydrological modelling. In addition, the *primary variables*, precipitation, mean

temperature and diurnal temperature range, are derived entirely from observed station data and represent a good independent dataset for evaluation of regional climate models and satellite derived products. The mean temperature fields are not suitable for climate change detection because the input dataset includes stations that have an urban warming bias. The *secondary variable* fields, wet-day frequency, vapour pressure, cloud cover and ground-frost frequency were constructed using a combination of observed data and empirical relationships with the primary variables. Therefore, these secondary variables should be used with caution in such climatological applications. Nonetheless, the secondary variables provide, for the first time, a century long record of spatially complete data.

For the primary variables, a direct consequence of the anomaly interpolation methodology is relaxation of the monthly fields towards the 1961-1990 mean in regions where there are no stations within the correlation decay distance. This occurs most often in earlier years, particularly for diurnal temperature range. To provide an indication of where this occurs, each monthly field has a companion field listing the distance to from each grid-centre to the nearest station.

Diurnal temperature range can be used in combination with mean temperature to calculate grids of maximum and minimum temperature. The resulting gridded time-series will include all of the variability contained in the mean temperature grids (nearly complete coverage in space-time) plus additional variability in diurnal temperature range where data are present. In domains where monthly diurnal temperature range is relaxed to the climatology, maximum and minimum temperature will only reflect variability in mean temperature.

For the secondary variables, the interpolation of merged station and synthetic data makes it more difficult to provide an indication of where a monthly field is based on (i) observed data, (ii) synthetic data derived from primary variables *with* inter-annual variability or (iii) synthetic data derived from primary variables that had been relaxed to the climatology. However, as with the primary variables, companion grids of grid-point to nearest station distances were calculated. If these are used in combination with the station information for the primary variable that were used to derive the synthetic grids, some idea of the contributing inputs can be obtained. For a more qualitative indication, the maps station distributions in Figures 1-3 (primary variables) and 10-12 (secondary variables) can be used.

The CRU05 dataset is available from the Climatic Research Unit, via Dr. David Viner (d.viner@uea.ac.uk) Climate Impacts LINK Project (<http://www.cru.uea.ac.uk/link>).

Acknowledgements: This work was undertaken with funding for MN from the UK Natural Environment Research Council (Grant No. GR3/09721) and MH from UK Department of the Environment, Transport and the Regions (DETR; Contract EPG 1/1/48). The CRU precipitation, mean temperature and diurnal temperature range datasets have been compiled over a number of years with support from the UK DETR and the US Department of Energy. Data obtained from the Global Historical Climatology Network and the Carbon Dioxide Information Analysis Centre supplemented the CRU archives. Other data supplied by numerous National Meteorological Agencies, research organisations and private individuals made this research possible and these contributions, while too numerous to mention by name, are gratefully acknowledged. Mike Hutchinson kindly supplied the interpolation software. The Climate Impacts LINK Project (UK DETR Contract EPG 1/1/16) at the Climatic Research Unit provided computing facilities for this research.

5. References

- Carter, T. R., M. L. Parry, H. Harasawa and S. Nishioka, 1994: *IPCC technical guidelines for assessing climate change impacts and adaptations*. University College, London and Centre for Global Environmental Research, Tsukuba.
- Christensen, J. H., B. Machehauer, R. G. Jones, C. Schar, P. M. Ruti, M. Castro and G. Visconti, 1997: Validation of present-day regional climate simulations over Europe: LAM simulations with observed boundary conditions. *Climate Dyn.*, **13**, 489-506.
- Cramer, W. and A. Fischer, 1996: Data requirements for global terrestrial ecosystem modelling. *Global Change and Terrestrial Ecosystems*, B. Walker and W. Steffen, Ed(s)., Cambridge University Press, 530-565.
- Dai, A., I. Fung and A. D. Del Genio, 1997a: Surface observed global land precipitation variations during 1900-1988. *J. Climate*, **11**, 2943-2962.
- Dai, A. and I. Y. Fung, 1993: Can climate variability contribute to the "missing" carbon sink? *Glob. Biogeochem. Cycl.*, **7**, 599-609.
- Dai, A. G., A. D. Del Genio and I. Y. Fung, 1997b: Clouds, precipitation and temperature range. *Nature*, **386**, 665-666.

- Diaz, H. F., R. S. Bradley and J. K. Eischeid, 1989: Precipitation fluctuations over global land areas since the late 1800s. *J. Geoph. Res. - Atmos.*, **94**, 1195-1210.
- Easterling, D. R., B. Horton, P. D. Jones, T. C. Peterson, T. R. Karl, D. E. Parker, M. J. Salinger, V. Razuvayev, N. Plummer, P. Jamason and C. K. Folland, 1997: Maximum and minimum temperature trends for the globe. *Science*, **277**, 364-367.
- Eischeid, J. K., H. F. Diaz, R. S. Bradley and P. D. Jones, 1991: *A comprehensive precipitation data set for global land areas*. DOE/ER-6901T-H1, US Department of Energy, Washington DC.
- Emerson, J. D. and D. C. Hoaglin, 1983: Resistant lines for y versus x. *Understanding robust and exploratory data analysis*, D. C. Hoaglin, F. Mosteller and J. W. Tukey, Ed(s)., Wiley.
- Groisman, P. Y., V. V. Koknaeva, T. A. Belokrylova and T. R. Karl, 1991: Overcoming biases of precipitation measurement: a history of the USSR experience. *Bull. Amer. Meteor. Soc.*, **72**, 1725-1733.
- Hahn, C. J., S. G. Warren and J. London, 1994: *Climatological data for clouds over the globe from surface observations, 1982-1991: the total cloud edition*. Report No., NDP026A, Carbon Dioxide Analysis Center, Oak Ridge National Laboratory, Oak Ridge, USA.
- Hansen, J. and S. Lebedeff, 1987: Global trends of measured surface air-temperature. *J. Geoph. Res. - Atmos.*, **92**, 13345-13372.
- Horton, B., 1995: Geographical distribution of changes in maximum and minimum temperatures. *Atm. Res.*, **37**, 101-117.
- Hulme, M., 1992: A 1951-80 global land precipitation climatology for the evaluation of General Circulation Models. *Climate Dyn.*, **7**, 57-72.
- Hulme, M., 1994: Global changes in precipitation in the instrumental period. *Global precipitation and climate change*, M. Desbois and F. Desalmand, Ed(s)., Springer-Verlag, 387-405.
- Hulme, M., J. Jones and M. G. New, in preparation: Representing 20th century space-time precipitation variability. An intercomparison of global precipitation climatologies. *J. Climate*.
- Hutchinson, M. F., 1995a: Interpolating mean rainfall using thin plate smoothing splines. *Int. J. Geog. Inf. Sys.*, **9**, 385-403.

- Hutchinson, M. F., 1995b: Stochastic space-time weather models from ground-based data. *Agric. Forest. Meteor.*, **73**, 237-264.
- Hutchinson, M. F. and P. E. Gessler, 1994: Splines - more than just a smooth interpolator. *Geoderma*, **62**, 45-67.
- Jones, P. D., 1994: Hemispheric surface air temperature variability - a reanalysis and update to 1993. *J. Climate*, **7**, 1794-1802.
- Jones, P. D. and M. Hulme, 1996: Calculating regional climatic time series for temperature and precipitation: methods and illustrations. *Int. J. Climatol.*, **16**, 361-377.
- Jones, P. D., M. New, D. E. Parker and S. Martin, submitted: Surface air temperature and its changes over the past 150 years. *Rev. Geophys.*
- Jones, P. D., T. J. Osborn and K. R. Briffa, 1997: Estimating sampling errors in large scale temperature averages. *J. Climate*, **10**, 2548-2568.
- Karl, T. R., P. D. Jones, R. W. Knight, G. Kukla, N. Plummer, V. Razuvayev, K. P. Gallo, J. Lindsey, R. J. Charlson and T. C. Peterson, 1993: A new perspective on recent global warming - asymmetric trends of daily maximum and minimum temperature. *Bull. Amer. Meteor. Soc.*, **74**, 1007-1023.
- Kimball, J. S., S. W. Running and R. Nemani, 1997: An improved method for estimating surface humidity from daily minimum temperature. *Agric. Forest. Meteor.*, **85**, 87-98.
- New, M. G., M. Hulme and P. D. Jones, in press: Representing 20th century space-time climate variability. I: Development of a 1961-1990 mean monthly terrestrial climatology. *J. Climate*.
- Piper, S. C. and E. F. Stewart, 1996: A gridded global data set of daily temperature and precipitation for terrestrial biosphere modeling. *Glob. Biogeochem. Cycl.*, **10**, 757-782.
- Ruschy, D. L., D. G. Baker and R. H. Skaggs, 1991: Seasonal-variation in daily temperature ranges. *J. Climate*, **4**, 1211-1216.
- Shuttleworth, J. W., 1992: Evaporation. *Handbook of Hydrology*, D. R. Maidment, Ed(s), McGraw-Hill, 4.1-4.53.

- Victoria, R. L., L. A. Martinelli, J. M. Moraes, M. V. Ballester, A. V. Krusche, G. Pellegrino, R. M. B. Almeida and J. E. Richey, 1998: Surface air temperature variations in the Amazon region and its borders during this century. *J. Climate*, **11**, 1105-1110.
- Wahba, G., 1990: *Spline models for observational data*. Society for Industrial and Applied Mathematics, 169pp.
- Wang, W. C., Q. Y. Zhang, D. R. Easterling and T. R. Karl, 1993: Beijing cloudiness since 1875. *J. Climate*, **6**, 1921-1927.
- Xie, P. and P. A. Arkin, 1996: Analyses of global monthly precipitation using gauge observations, satellite estimates and numerical model predictions. *J. Climate*, **9**, 840-858.
- Xie, P. P., B. Rudolf, U. Schneider and P. A. Arkin, 1996: Gauge-based monthly analysis of global land precipitation from 1971 to 1994. *J. Geoph. Res. - Atmos.*, **101**, 19023-19034.

6. Figure Captions

Figure 1. Distribution of precipitation stations in the CRU dataset for the indicated years. Shaded areas show 0.5° grid cells that have a station within 450km of the cell centre.

Figure 2. Distribution of mean temperature stations in the CRU dataset for the indicated years. Shaded areas show 0.5° grid cells that have a station within 1200km of the cell centre.

Figure 3. Distribution of diurnal temperature range stations in the CRU dataset for the indicated years. Shaded areas show 0.5° grid cells that have a station within 750km of the cell centre.

Figure 4. Zonally averaged monthly correlation decay distances (CDDs) for precipitation (solid), mean temperature (dots) and diurnal temperature range (dashes).

Figure 5. Geographical tiles used for the interpolation of monthly precipitation anomalies from station data. Fewer tiles were used for mean temperature and diurnal temperature range because there were not as many stations with data for these variables.

Figure 6. Regional time-series of annual precipitation anomalies (relative to 1961-1990 average), and their 20-year running standard deviations, over the Amazon basin (top) and the UK (bottom). Both DAI and CRU05 were masked using the HULME grid – see text for details. Solid = HULME, dotted = DAI and dashed = CRU05. The thin lines in the upper panel represent the number of grid-points contributing to the HULME (solid) and DAI (dotted) time-series. The grey curve in the top right plot represents the mean of the running CVs of stations in the CRU dataset that fall within the Amazon window (see text for details).

Figure 7. Regional time-series of annual temperature anomalies (relative to 1961-1990 average), and their 20-year running standard deviations, over the Amazon basin (top) and the UK (bottom). The series were derived in the same manner to Figure 6 (see text for details). Solid = JONES, dotted = CRU05; thick = time series, thin = station or grid-box counts.

Figure 8. Time series of annual temperature anomalies (relative to 1961-1990 average) for (top) global land areas excluding Antarctica, (middle) Northern Hemisphere land areas and (bottom) Southern

Hemisphere land areas excluding Antarctica. In each case the left panel contains the time series (solid = JONES, dotted = CRU05 using JONES mask, dashed = CRU05 with complete coverage) and the right the difference between CRU05 and JONES (dotted = CRU05 masked minus JONES; dashed = CRU05-unmasked minus JONES). The shaded area represents ± 1 standard error of the JONES time series (see text and Jones *et al.* 1997 for details).

Figure 9. Time series of annual diurnal temperature range anomalies (relative to 1961-1990 average) for the Northern Hemisphere from CRU05 and EAST (top panel; solid = CRU05; dotted = EAST) and the difference between the two series (bottom panel).

Figure 10. Distribution of cloud cover stations in the CRU dataset for the indicated years. Shaded areas show 0.5° grid cells that have a station within 750km of the cell centre.

Figure 11. Distribution of vapour pressure stations in the CRU dataset for the indicated years. Shaded areas show 0.5° grid cells that have a station within 1000km of the cell centre.

Figure 12. Distribution of wet-day frequency stations in the CRU dataset for the indicated years. Shaded areas show 0.5° grid cells that have a station within 400km of the cell centre.

Figure 13. Zonally averaged monthly correlation decay distances for cloud cover (solid), wet-day frequency (dots) and vapour pressure (dashes).

Figure 14. Strength of correlation between monthly cloud cover and the two primary variables, diurnal temperature range (top) and precipitation (bottom). Positive and negative correlations are black and white respectively.

Figure 15. Example of data points used in the interpolation of cloud cover anomalies. Pluses and dots represent real station data and data extracted from the gridded synthetic anomaly fields derived from diurnal temperature range respectively.

Figure 16. Correlation (Pearson's r) between station time-series of observed and synthetic vapour pressure, calculated using dew point temperature estimated from minimum temperature. Station data

were converted to anomalies and grouped into 5° lat/lon bins before the calculation of the correlation coefficient.

Figure 17. Example of the relationship used to predict wet-day frequency from monthly precipitation for a station in the UK.

Figure 18. Correlation between observed wet-day frequency station time-series and those predicted using precipitation.

Figure 19. Validation statistics for the relationship used to predict wet-day frequency from monthly precipitation. Left: predicted-observed errors as a function of observed monthly wet-day frequency. Right: range of predicted-observed correlation coefficients for stations in the CRU wet-day frequency dataset. Thick line = median, medium lines = quartiles and thin lines = ten percentiles.

Figure 20. Validation statistics for the prediction of monthly ground-frost frequency using monthly minimum temperature at 120 stations in the UK. Left: predicted-observed errors as a function of observed ground-frost frequency. Right: distribution of predicted-observed correlations at individual stations. Thick line = median, medium lines = upper and lower quartiles and thin lines = 10th and 90th percentiles. In summer months where quartiles and percentiles are not shown, there were not enough stations with frost occurrence to permit their calculation.

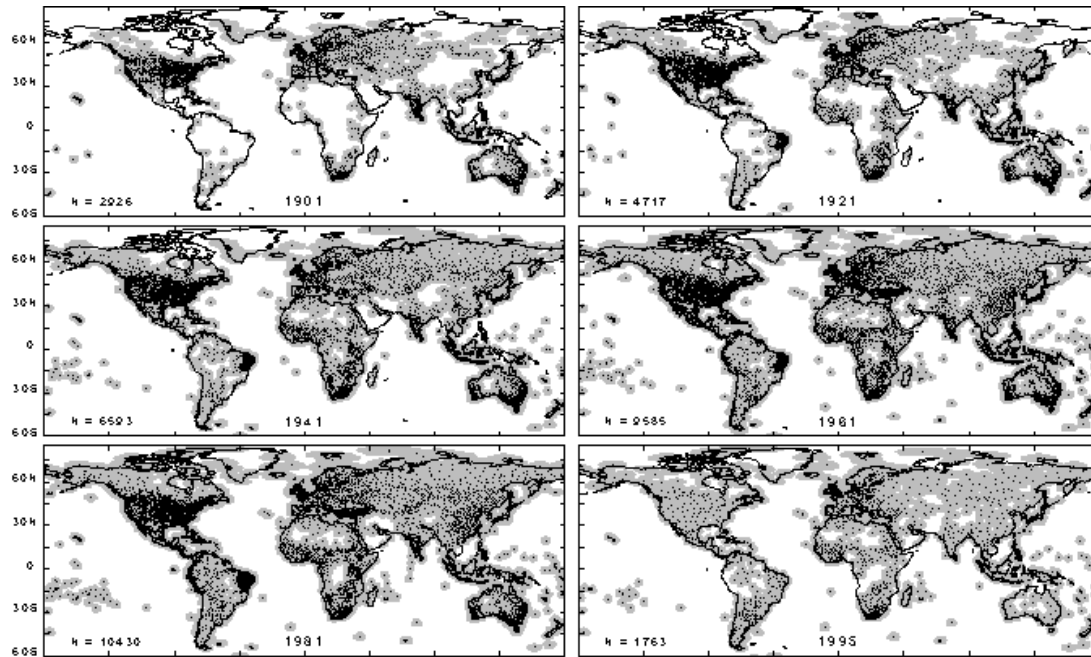


Figure 1. Distribution of precipitation stations in the CRU dataset for the indicated years. Shaded areas show 0.5° grid cells that have a station within 450km of the cell centre.

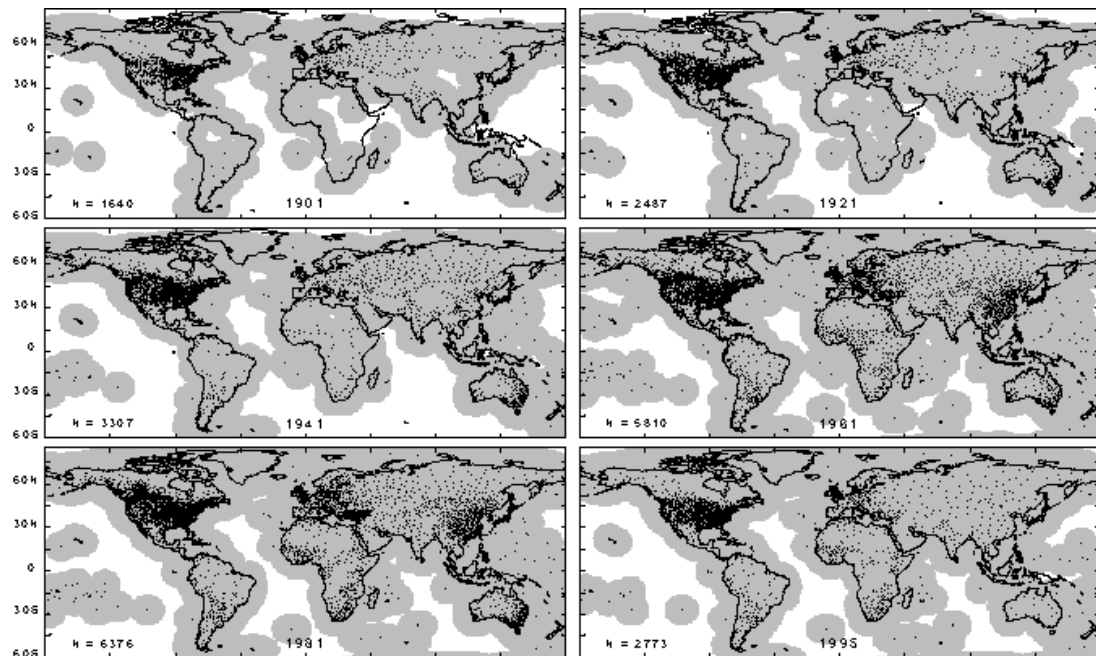


Figure 2. Distribution of mean temperature stations in the CRU dataset for the indicated years. Shaded areas show 0.5° grid cells that have a station within 1200km of the cell centre.

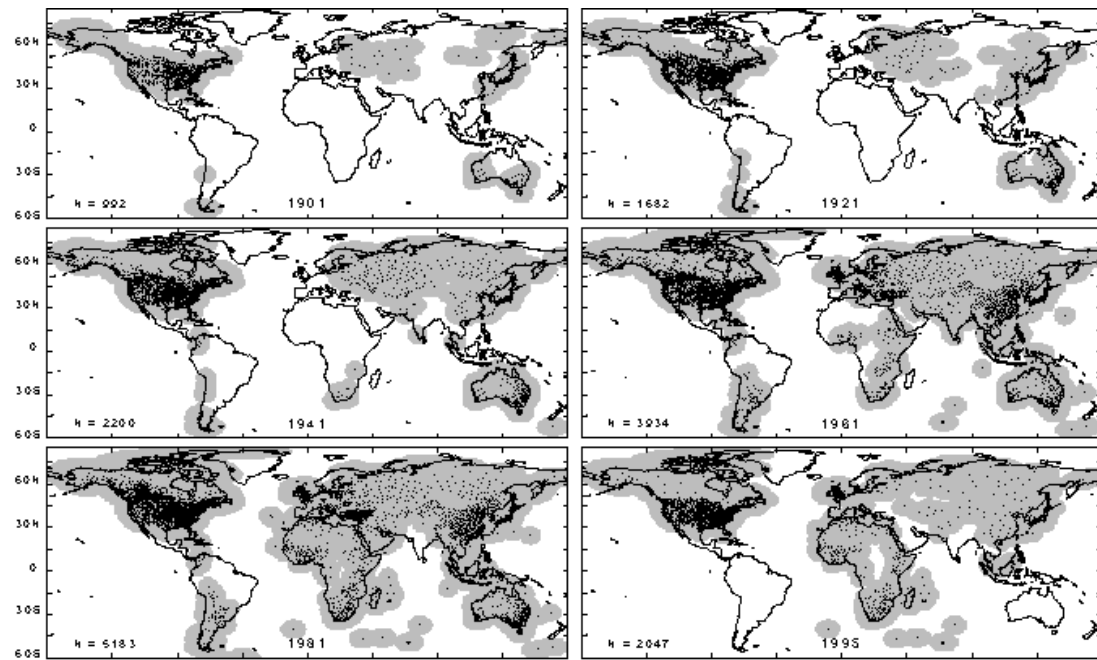


Figure 3. Distribution of diurnal temperature range stations in the CRU dataset for the indicated years.

Shaded areas show 0.5° grid cells that have a station within 750km of the cell centre.

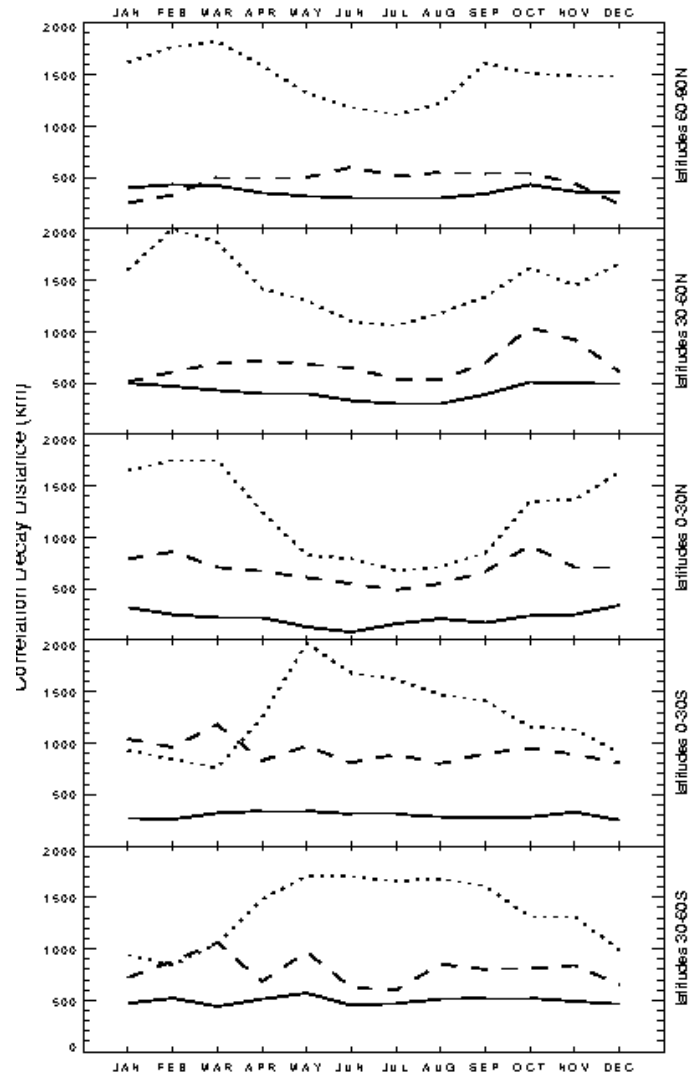


Figure 4. Zonally averaged monthly correlation decay distances (CDDs) for precipitation (solid), mean temperature (dots) and diurnal temperature range (dashes).

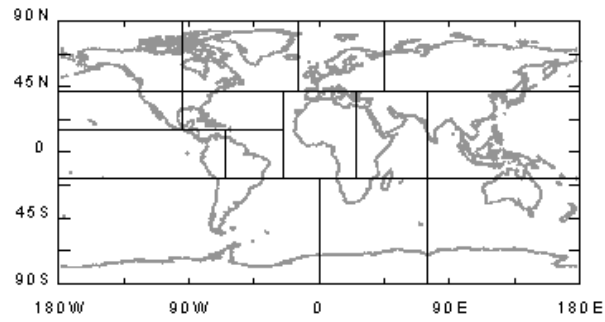


Figure 5. Geographical tiles used for the interpolation of monthly precipitation anomalies from station data. Fewer tiles were used for mean temperature and diurnal temperature range because there were not as many stations with data for these variables.

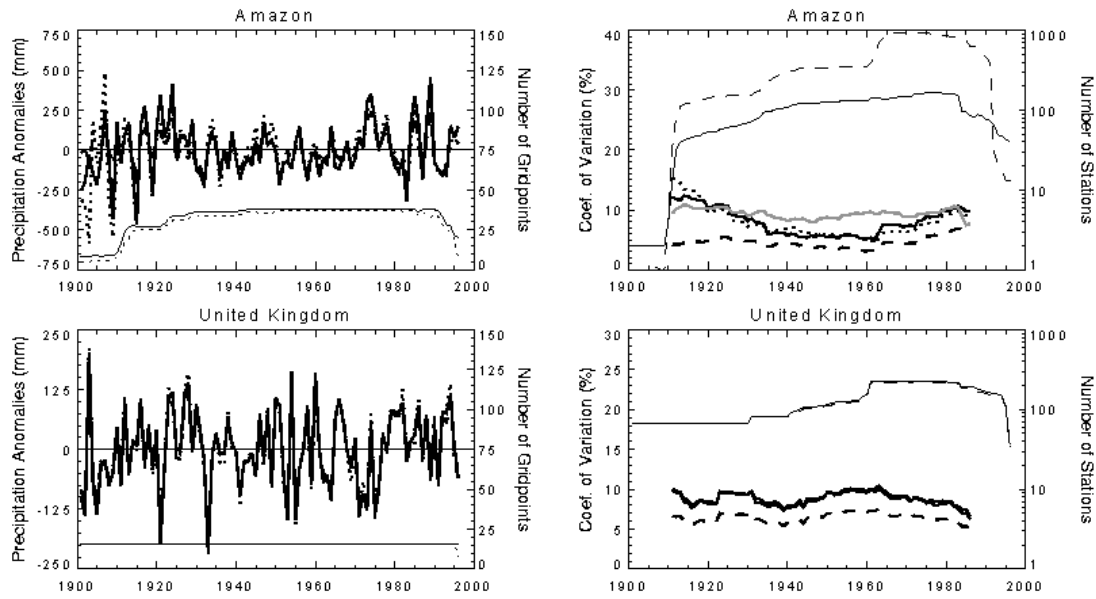


Figure 6. Regional time-series of annual precipitation anomalies (relative to 1961-1990 average), and their 20-year running standard deviations, over the Amazon basin (top) and the UK (bottom). Both DAI and CRU05 were masked using the HULME grid – see text for details. Solid = HULME, dotted = DAI and dashed = CRU05. The thin lines in the upper panel represent the number of grid-points contributing to the HULME (solid) and DAI (dotted) time-series. The grey curve in the top right plot represents the mean of the running CVs of stations in the CRU dataset that fall within the Amazon window (see text for details).

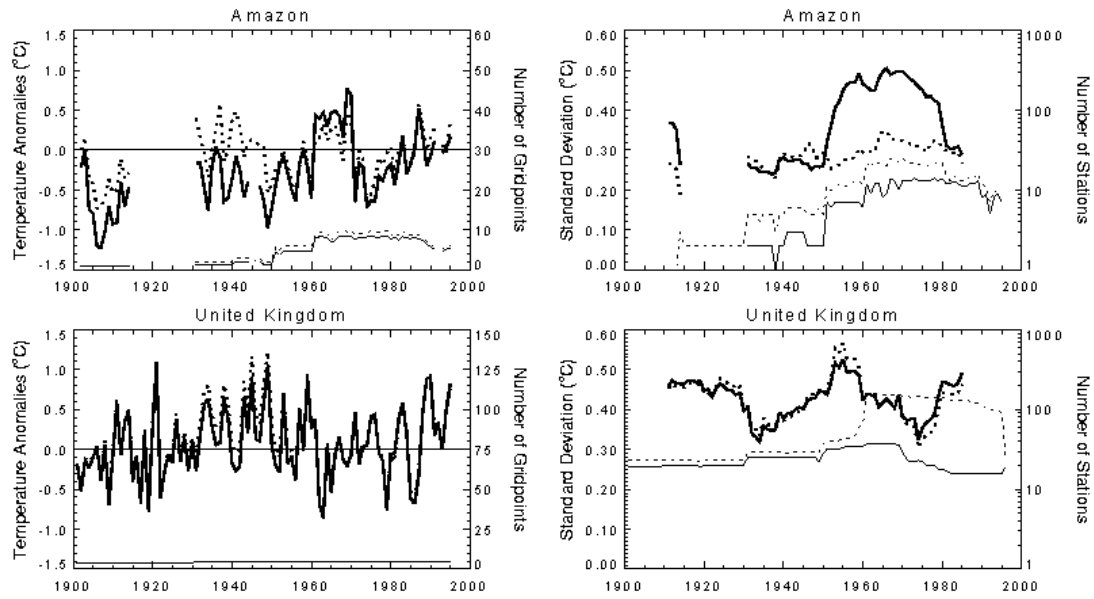


Figure 7. Regional time-series of annual temperature anomalies (relative to 1961-1990 average), and their 20-year running standard deviations, over the Amazon basin (top) and the UK (bottom). The series were derived in the same manner to Figure 6 (see text for details). Solid = JONES, dotted = CRU05; thick = time series, thin = station or grid-box counts.

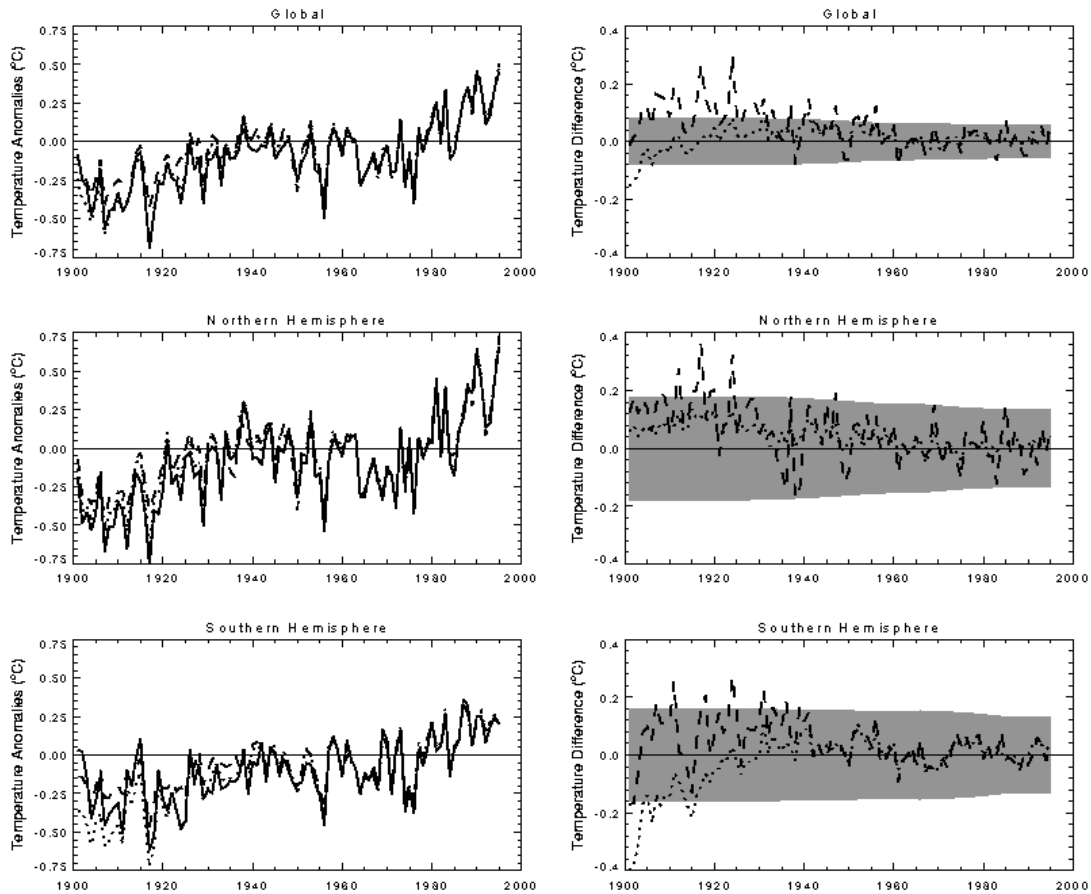


Figure 8. Time series of annual temperature anomalies (relative to 1961-1990 average) for (top) global land areas excluding Antarctica, (middle) Northern Hemisphere land areas and (bottom) Southern Hemisphere land areas excluding Antarctica. In each case the left panel contains the time series (solid = JONES, dotted = CRU05 using JONES mask, dashed = CRU05 with complete coverage) and the right panel the difference between CRU05 and JONES (dotted = CRU05 masked minus JONES; dashed = CRU05-unmasked minus JONES). The shaded area represents ± 1 standard error of the JONES time series (see text and Jones *et al.* 1997 for details).

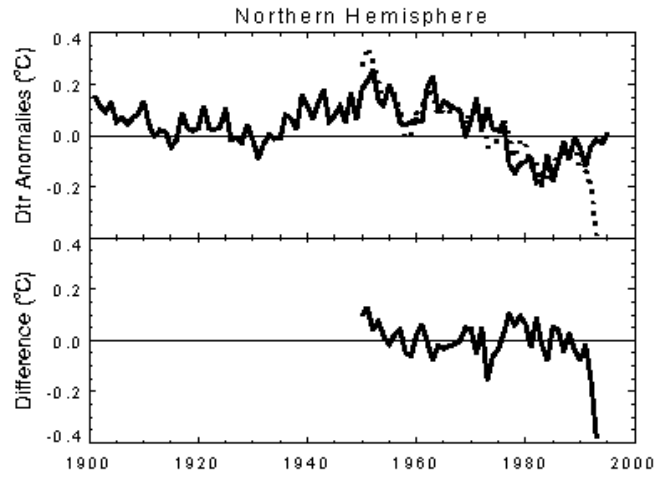


Figure 9. Time series of annual diurnal temperature range anomalies (relative to 1961-1990 average) for the Northern Hemisphere from CRU05 and EAST (top panel; solid = CRU05; dotted = EAST) and the difference between the two series (bottom panel).

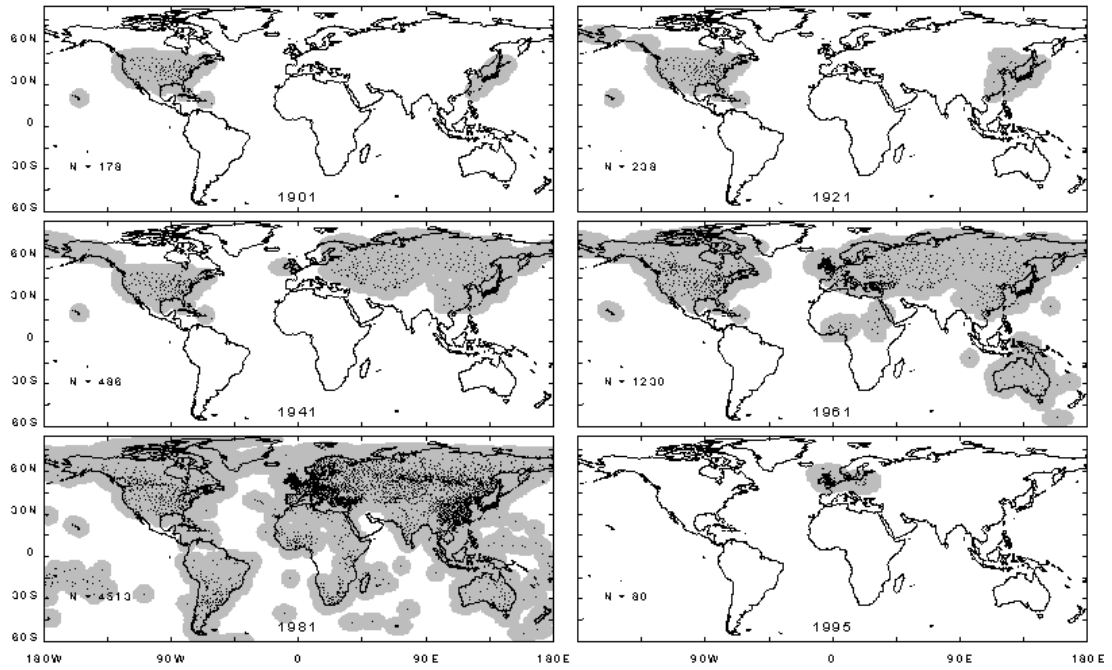


Figure 10. Distribution of cloud cover stations in the CRU dataset for the indicated years. Shaded areas show 0.5° grid cells that have a station within 750km of the cell centre.

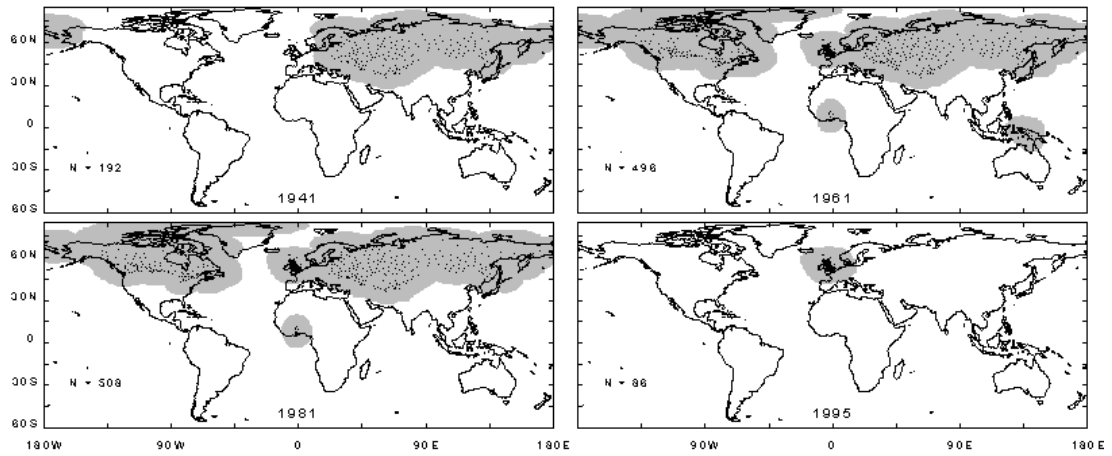


Figure 11. Distribution of vapour pressure stations in the CRU dataset for the indicated years. Shaded areas show 0.5° grid cells that have a station within 1000km of the cell centre.

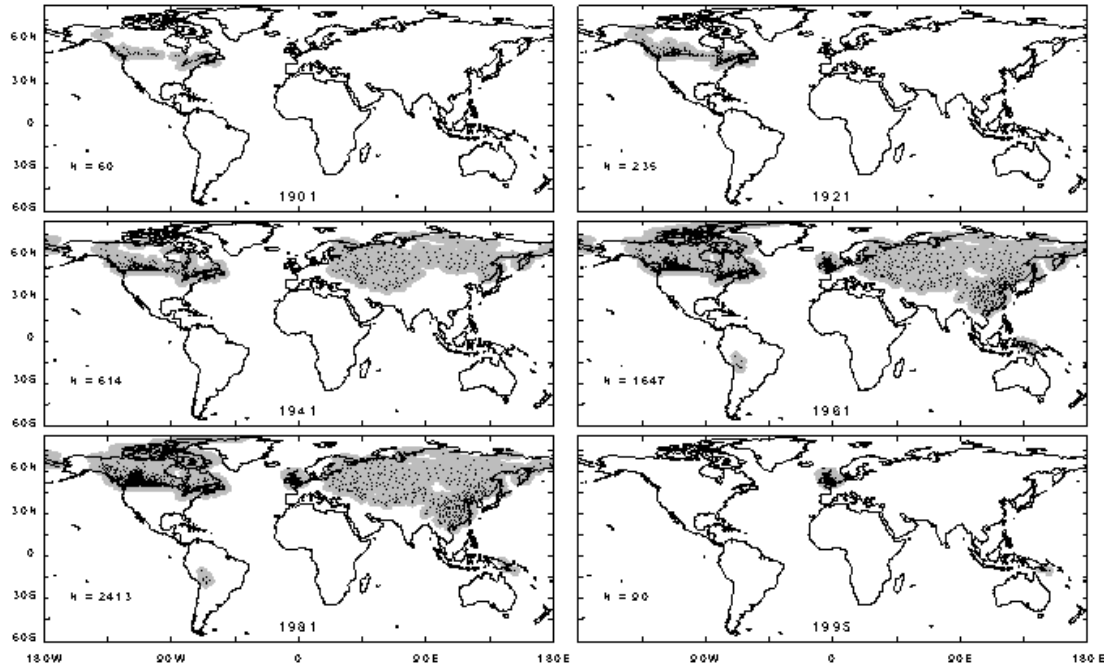


Figure 12. Distribution of wet-day frequency stations in the CRU dataset for the indicated years. Shaded areas show 0.5° grid cells that have a station within 400km of the cell centre.

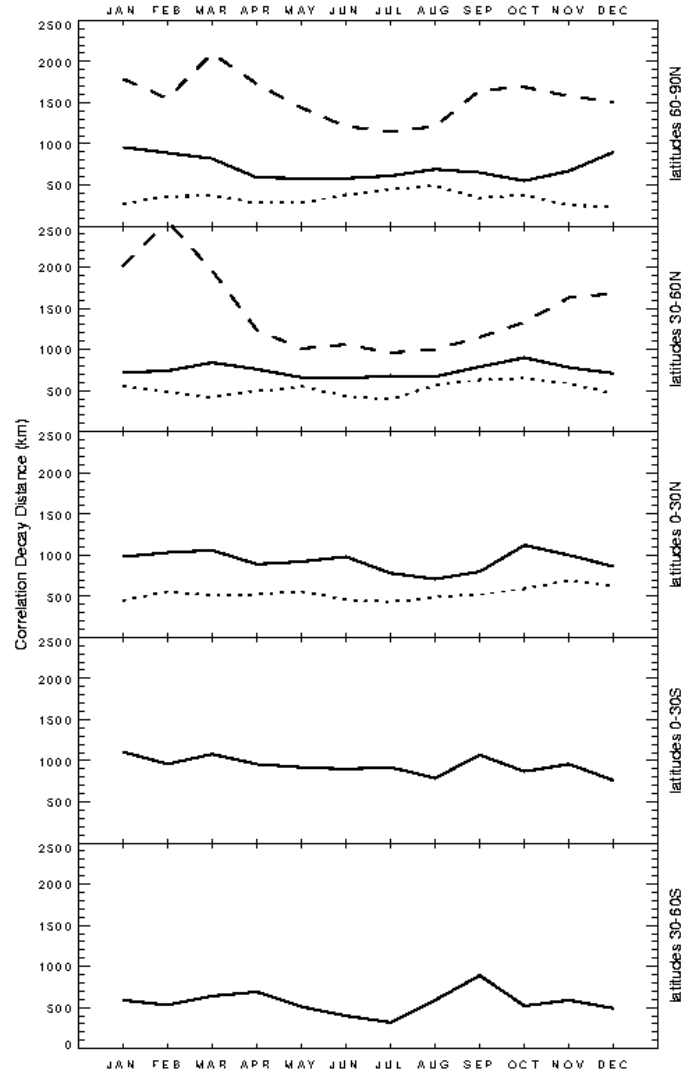
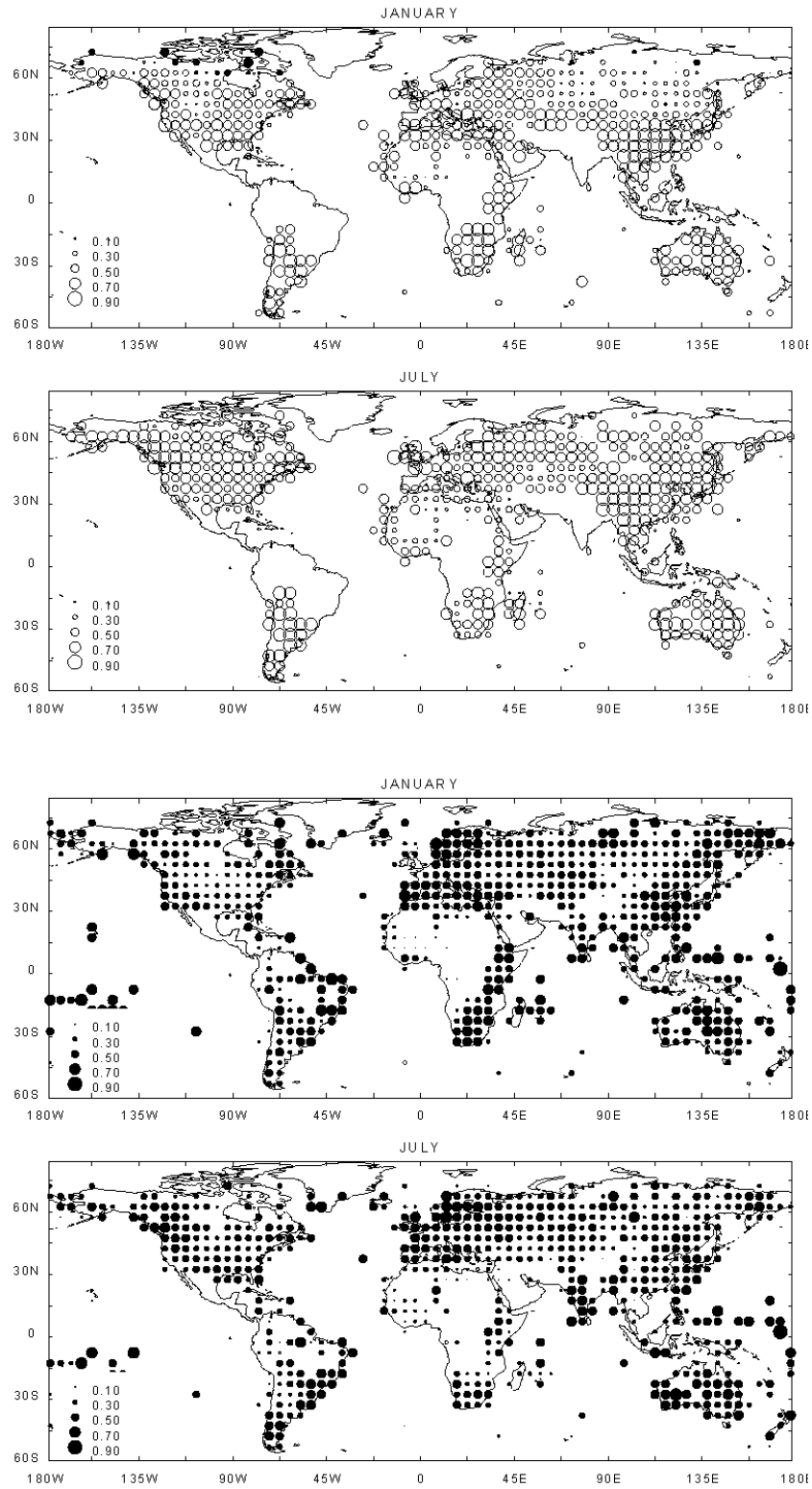


Figure 13. Zonally averaged monthly correlation decay distances for cloud cover (solid), wet-day frequency (dots) and vapour pressure (dashes).



14. Strength of correlation between monthly cloud cover and the two primary variables, diurnal

white respectively.

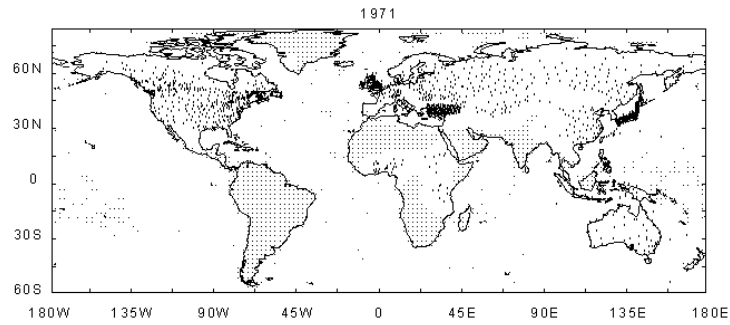


Figure 15. Example of data points used in the interpolation of cloud cover anomalies. Pluses and dots represent real station data and data extracted from the gridded synthetic anomaly fields derived from diurnal temperature range respectively.

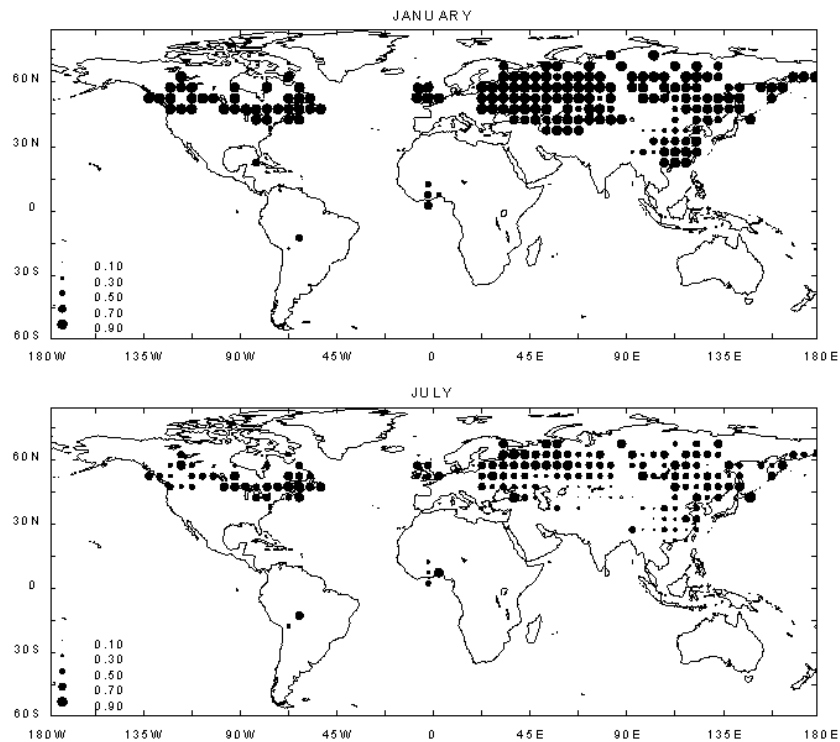


Figure 16. Correlation (Pearson's r) between station time-series of observed and synthetic vapour pressure, calculated using dew point temperature estimated from minimum temperature. Station data were converted to anomalies and grouped into 5° lat/lon bins before the calculation of the correlation coefficient.

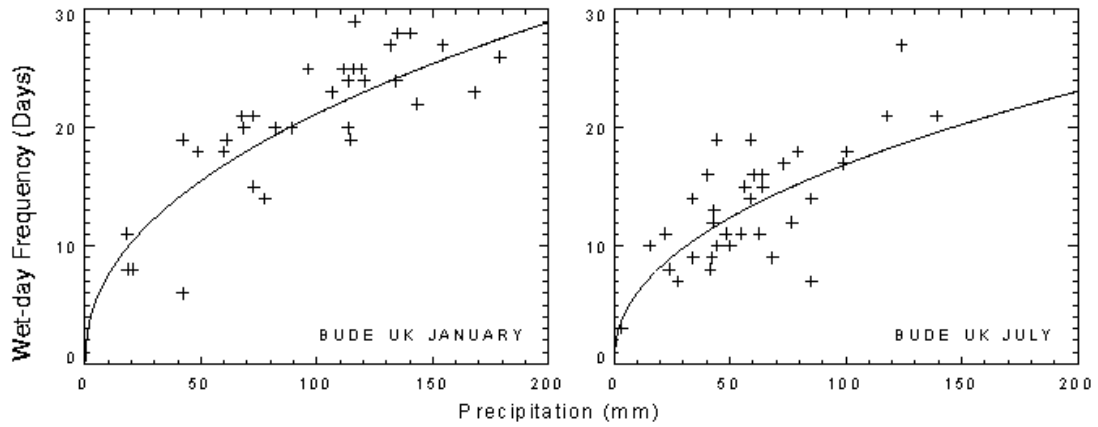


Figure 17. Example of the relationship used to predict wet-day frequency from monthly precipitation for a station in the UK.

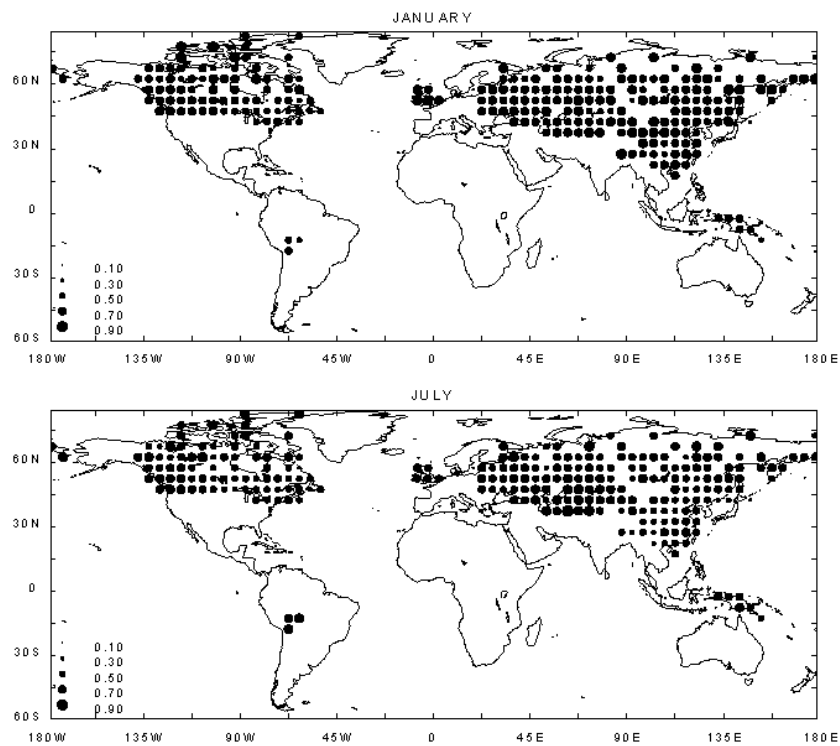


Figure 18. Correlation between observed wet-day frequency station time-series and those predicted using precipitation.

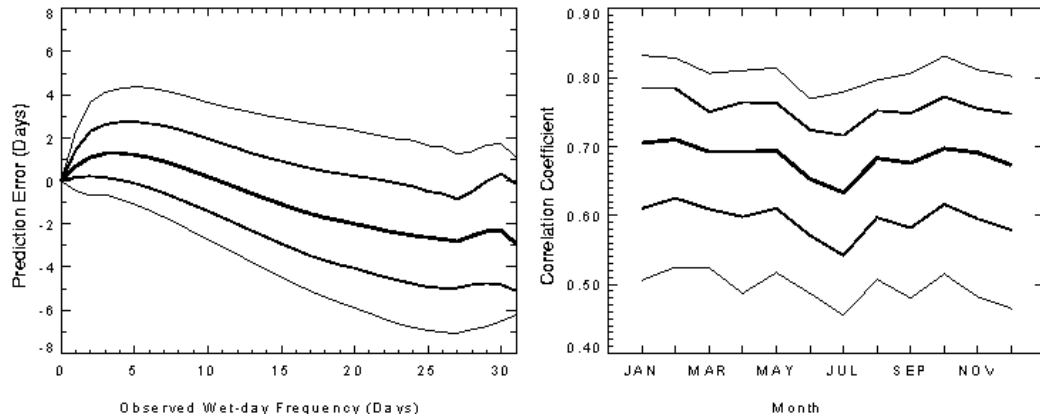


Figure 19. Validation statistics for the relationship used to predict wet-day frequency from monthly precipitation. Left: predicted-observed errors as a function of observed monthly wet-day frequency. Right: range of predicted-observed correlation coefficients for stations in the CRU wet-day frequency dataset. Thick line = median, medium lines = quartiles and thin lines = ten percentiles.

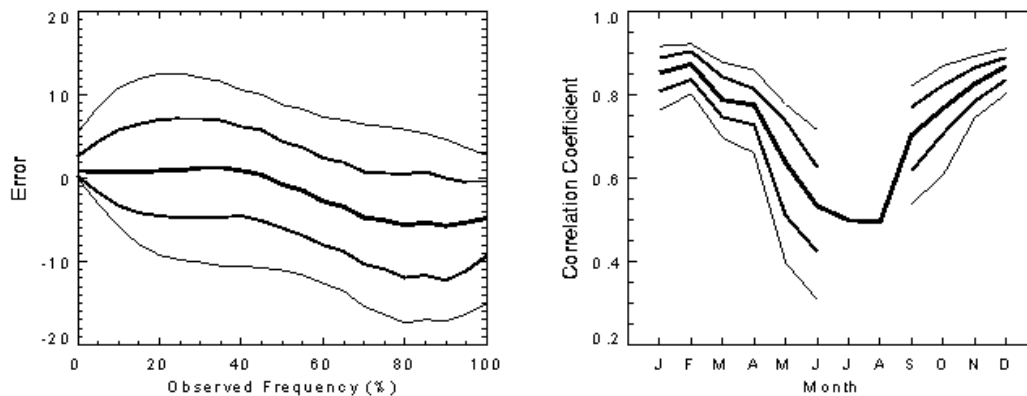


Figure 20. Validation statistics for the prediction of monthly ground-frost frequency using monthly minimum temperature at 120 stations in the UK. Left: predicted-observed errors as a function of observed ground-frost frequency. Right: distribution of predicted-observed correlations at individual stations. Thick line = median, medium lines = upper and lower quartiles and thin lines = 10th and 90th percentiles.